Path Instability of a Rising Bubble

Guillaume Mougin and Jacques Magnaudet
Institut de Mécanique des Fluides de Toulouse, UMR CNRS-INPT-UPS 5502,
2, allée du Professeur Camille Soula, 31400 Toulouse, France
(Received 10 July 2001; published 19 December 2001)

We model the problem of path instability of a rising bubble by considering the bubble as a spheroidal body of fixed shape, and we solve numerically the coupled fluid-body problem. Numerical results show that this model exhibits path instability for large enough values of the control parameters. The corresponding characteristics of the zigzag and spiral paths are in good agreement with experimental observations. Analysis of the vorticity field behind the bubble reveals that a wake instability leading to a double threaded wake is the primary cause of the path instability.

DOI: 10.1103/PhysRevLett.88.014502 PACS numbers: 47.55.Dz, 47.20.Ky, 47.27.Vf

Many experiments performed over the last 50 years have demonstrated that millimetric bubbles rising in low-viscosity liquids do not generally follow a straight trajectory [1]. In the regime where bubbles exhibit approximately oblate spheroidal shapes, they rather rise in zigzag within a given vertical plane or spiral around a vertical axis. In pure water the transition from straight path to zigzag path occurs when the equivalent diameter of the bubble exceeds 1.8 mm, which corresponds to a rise Reynolds number of about 660 and an aspect ratio about 1.85 [2]. Nevertheless, tiny quantities of surface-active agents suffice to lower dramatically the critical Reynolds number, and values down to 200 have frequently been reported. Several theoretical approaches have been attempted to understand the origin of the transition from straight path to zigzag or spiral path. Owing to the large value of the rise Reynolds number, most of them described the flow past the bubble as irrotational and took into account effects of gravity, surface tension, and liquid inertia to determine the bubble shape in such a way that the condition of constant pressure within the bubble is satisfied at any time. Unfortunately, predictions of these theories conflict severely with experimental evidence. For instance, spiral paths with pitch and diameter close to those observed experimentally may be predicted, provided a substantial drift angle exists between the rise velocity and the minor axis of the bubble [3]. However, detailed measurements prove that this angle is almost zero all along the path [4]. Saffman [5] used similar assumptions to determine the flow and bubble shape near the front stagnation point and concluded that the rectilinear motion becomes unstable when the aspect ratio of the bubble exceeds 1.2. He then suggested existence of a wake behind the bubble and conjectured that the instability of the rectilinear motion may trigger the instability of the wake. Recent experiments have indeed demonstrated that, under certain conditions, oblate spheroidal bubbles are followed by an open wake (see [1]), even in the absence of any contamination of the bubble surface by surfactants [6]. The dynamics of this wake may have a crucial effect on the path of the bubble, as periodic vortex shedding has been proved to have on the path of two-dimensional bubbles rising in a Hele-Shaw cell [7]. Therefore, in contrast with available theories, our goal in this Letter is to disregard any effect associated with the small-scale deformability of the bubble in order to determine whether the dynamics of the three-dimensional wake behind an oblate spheroidal bubble of fixed shape are sufficient to explain path instability and to produce zigzag and spiral paths with realistic geometrical characteristics.

We explore the possibility just described by solving numerically the unsteady three-dimensional incompressible Navier-Stokes equations in a large domain of fluid surrounding a fixed-shape bubble and we couple these equations with the force and torque balances that determine the motion of the bubble. Referring velocities to a fixed origin and to axes rotating at the same rate as the bubble, the Navier-Stokes equations take the form [8]

$$\nabla \cdot \boldsymbol{V} = 0,$$
$$\frac{\partial \boldsymbol{V}}{\partial t} + \Omega \times \boldsymbol{V} + \nabla \cdot [\boldsymbol{V}(\boldsymbol{V} - \boldsymbol{W})] = -\frac{1}{\rho}\nabla P + \nu \nabla^2 \boldsymbol{V}, \quad (1)$$

with $\boldsymbol{W} = \boldsymbol{U} + \Omega \times \boldsymbol{r}$, $\boldsymbol{r}$ being the current position measured from the geometrical center of the bubble whose velocity and rotation rate are $\boldsymbol{U}$ and Ω, respectively. Since we assume that the bubble behaves as a nondeformable body and is filled with a gas of negligible viscosity, its surface is submitted to an impermeability condition and a shear-free condition, namely

$$\boldsymbol{V} \cdot \boldsymbol{n} = \boldsymbol{W} \cdot \boldsymbol{n}, \qquad \boldsymbol{n} \times [(\nabla \boldsymbol{V} + {}^{T}\nabla \boldsymbol{V}) \cdot \boldsymbol{n}] = 0, \quad (2)$$

$\boldsymbol{n}$ being the unit normal to the surface. We assume $\boldsymbol{V} = \boldsymbol{0}$ on the upstream part of the fictitious outer boundary limiting the computational domain, and use an absorbing boundary condition on the downstream part of this boundary to allow velocity disturbances in the far wake to leave freely the numerical domain. During a time step of the resolution of (1),(2), $\boldsymbol{U}$ and Ω keep constant values. Then,

at the end of the time step, the motion of the bubble is deduced from the Kirchhoff equations which may be rigorously generalized to viscous flows [8,9]. Since the bubble is assumed to have zero inertia, these equations reduce to

$$\begin{aligned} \mathbb{A} \cdot \frac{d\boldsymbol{U}}{dt} &= \boldsymbol{F}_\omega - \rho \mathcal{V} \boldsymbol{g} - \Omega \times (\mathbb{A} \cdot \boldsymbol{U}), \\ \mathbb{D} \cdot \frac{d\Omega}{dt} &= \Gamma_\omega - \Omega \times (\mathbb{D} \cdot \Omega) - \boldsymbol{U} \times (\mathbb{A} \cdot \boldsymbol{U}), \end{aligned} \tag{3}$$

where $\boldsymbol{g}$ denotes gravity, $\mathcal{V}$ is the volume of the bubble, $\mathbb{A}$ and $\mathbb{D}$ are second-order diagonal added-mass tensors characterizing the inertia of the fluid set in motion by a translation and a rotation of the bubble, respectively, and $\boldsymbol{F}_\omega$ and Γ_ω are the instantaneous force and torque resulting from the existence of vorticity in the flow. The right-hand side of (3) is straightforwardly obtained at the end of the current time step by integrating the local stress and moment over the bubble surface. The components of $\mathbb{A}$ and $\mathbb{D}$ involved in the left-hand side are evaluated once and for all from irrotational flow theory at the very beginning of the computation because it is now established that added-mass tensors are not affected by finite-Reynolds-number effects [1,8,9]. Details about the numerical techniques involved in the resolution of (1)–(3) may be found in [8].

The two control parameters governing the physical problem are the Galileo number $\mathrm{Ga} = \|\boldsymbol{g}\|^{1/2} R_{\mathrm{eq}}{}^{3/2}/\nu$ and the aspect ratio $\chi = b/a$, $R_{\mathrm{eq}} = (ab^2)^{1/3}$ being the equivalent radius of the bubble whose major and minor axes have lengths b and a, respectively. Most numerical simulations reported below are carried out for $\mathrm{Ga} = 138$, corresponding to an air bubble with $R_{\mathrm{eq}} = 1.25$ mm rising in water under standard conditions. The bubble and the surrounding liquid are initially at rest; the bubble is then set in motion by buoyancy. A small sinusoidal perturbation lying in an arbitrary vertical plane and having a relative amplitude $\varepsilon = 10^{-4}$ and an arbitrary frequency is superposed to the gravity field to trigger the path instability.

Observed trajectories are represented in Fig. 1. Below a certain critical aspect ratio $\chi_c \approx 2.2$ the trajectory remains straight and vertical and the terminal velocity tends to a constant value resulting from a balance between buoyancy and viscous drag. Then, within a narrow range of aspect ratios, a plane zigzag with varying amplitude appears. Finally, a regular planar zigzag of constant amplitude is obtained for $\chi \geq 2.35$. As shown in Fig. 2(a), the saturated amplitude is almost independent of χ in the range $2.35 \leq \chi \leq 2.50$. It might well be that the bifurcation just described is subcritical, but additional computations are required to confirm this possibility. Another series of computations was carried out with χ maintained at the fixed value $\chi = 2.5$ and Ga varied in the range $20 < \mathrm{Ga} < 60$. As revealed by Fig. 2(b), the zigzag occurs beyond a threshold $\mathrm{Ga}_c \sim 30$; for $\mathrm{Ga} \leq 50$ its amplitude increases proportionally to $(\mathrm{Ga} - \mathrm{Ga}_c)^{1/2}$, a behavior typical of a supercritical Hopf bifurcation. Hence we conclude that the two transitions by which the zigzag stage can be reached

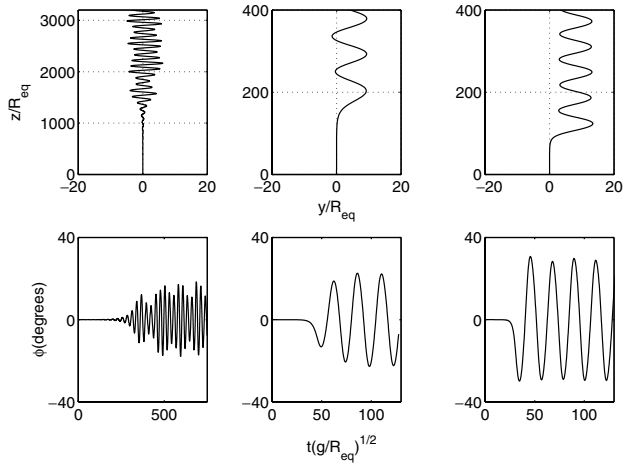

FIG. 1. Evolution of the path of a bubble with $\mathrm{Ga} = 138$. Top: Position of the geometric center; bottom: angle between the minor axis and the vertical direction. From left to right: $\chi = 2.30$, $\chi = 2.40$, $\chi = 2.50$.

have a different nature, depending on what control parameter is maintained fixed.

As soon as we detect the growth of the transverse motion, we change the plane perturbation applied to $\boldsymbol{g}$ into a rotating perturbation with a vertical axis, while keeping the amplitude and the frequency of this perturbation unchanged. The bubble goes on zigzagging, but its motion also develops a slowly growing component perpendicular to the plane of the zigzag. Then we switch off the perturbation. Ultimately, the two horizontal components of the motion reach identical magnitudes and the bubble goes on spiraling around the vertical axis, as shown in Fig. 3. It is worth mentioning that we also tried to trigger directly the spiraling mode by applying the rotational perturbation as soon as the bubble was released from rest. It turned out that the bubble selected a preferential plane within which it started zigzagging with the characteristics given above. Summarizing, the foregoing observations show that the system exhibits two symmetry breakings corresponding to the rectilinear/zigzag and zigzag/spiral transition, respectively. So far we have always observed that a zigzag path of constant amplitude eventually changes into a spiral. The zigzag is always observed first because its growth rate is much larger than

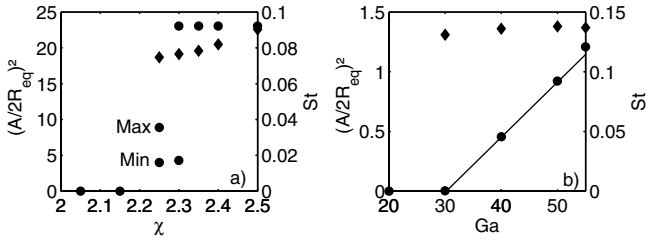

FIG. 2. Evolution of the relative amplitude $A/2R_{\mathrm{eq}}$ (●) and Strouhal number $\mathrm{St} = 2f(R_{\mathrm{eq}}/g)^{1/2}$ (◆) of the zigzag. Left: $\mathrm{Ga} = 138$, variable χ; right: $\chi = 2.5$, variable Ga.

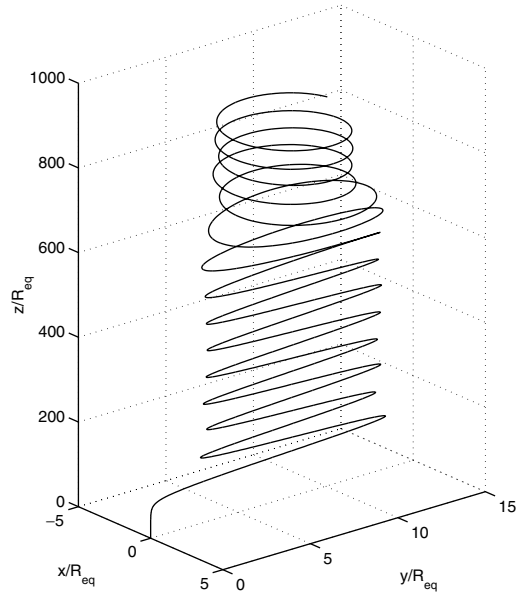

FIG. 3. Path of a zigzagging/spiraling bubble (Ga = 138, $\chi = 2.50$).

that of the spiral (Fig. 4). This scenario is consistent with experimental observations, since most authors detect only zigzagging paths, sometimes followed by a transition to a spiral path, while the reverse transition has never been reported (see [1]). For $\chi = 2.5$ and Ga = 138, we observe a saturated crest-to-crest amplitude $A/2R_{\mathrm{eq}}$ of the zigzag motion about 4.8, a Strouhal number $\mathrm{St} = 2f(R_{\mathrm{eq}}/g)^{1/2}$ based on the frequency f of the zigzag about 0.09, and a maximum angle θ_M between the path and the direction of gravity about 29°. In the spiral stage these values change to $A/(2R_{\mathrm{eq}}) = 3.1$, St = 0.108, and $\theta_S = 27°$. A compilation of experimental observations reported for both types of path indicates $A/2R_{\mathrm{eq}} \in [3.0, 4.0]$, $\mathrm{St} \in [0.10, 0.15]$, θ_M and $\theta_S \in [20°, 30°]$, which leads us to conclude that the predictions of our model are realistic.

Examination of the streamwise vorticity field plotted in Fig. 5 highlights the origin of the path instability and establishes a one-to-one correspondence between the wake structure and the nature of the path. While the wake is axisymmetric for $\chi < \chi_c$ [Fig. 5(a)], vorticity is shed downstream of the bubble under the form of a double threaded wake for $\chi > \chi_c$ [Figs. 5(b)–5(c)]. In the zigzag stage, the vorticity contained in the two counterrotating vortices changes sign twice during a period of the path, crossing zero when the curvature of the path vanishes. This is a clear indication of a strong coupling between the rotation of the bubble and the structure of its wake. In the spiraling stage [Fig. 5(c)] the two threads tend to wrap up around one another and the vorticity contained in each of them keeps a constant sign all along the trajectory. Similar wake structure has already been reported in recent experiments in the same range of Reynolds number [6]. The reason why varying χ has a direct effect on the wake structure follows directly from the fact that the local value of the surface vorticity on a curved shear-free surface is twice the product of the curvature by the tangential velocity [10]. Using this argument it can be shown that for large values of χ, the maximum vorticity on a spheroidal bubble of imposed aspect ratio increases as $\chi^{8/3}$ for large Reynolds numbers, so that the maximum vorticity corresponding to $\chi = 2.50$ is about 20% larger than that corresponding to $\chi = 2.30$. Based on this remark, the following physical scenario may be proposed for explaining the evolution of the whole system. For small enough aspect ratios, the amount of vorticity generated on the bubble surface is moderate and can be evacuated downstream under the form of an axisymmetric wake by the combined action of viscous diffusion and axisymmetric transport. Beyond a certain critical aspect ratio $\chi_c(\mathrm{Ga})$, the above mechanism is no longer sufficiently efficient because too much vorticity is generated at the bubble surface. Then the axisymmetric wake becomes unstable and breaks into a double-threaded open wake. In the zigzag configuration, the amount of vorticity shed downstream is still limited by the fact that the double-threaded structure vanishes twice during a period of the motion. Consequently, the spiral path emerges eventually

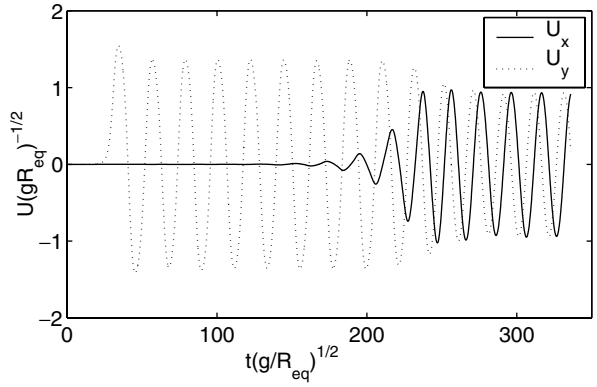

FIG. 4. Evolution of the two horizontal components of the bubble velocity (Ga = 138, $\chi = 2.50$); the rotating perturbation has been introduced at $t(g/R_{\mathrm{eq}})^{1/2} \approx 40$ and switched off at $t(g/R_{\mathrm{eq}})^{1/2} \approx 170$.

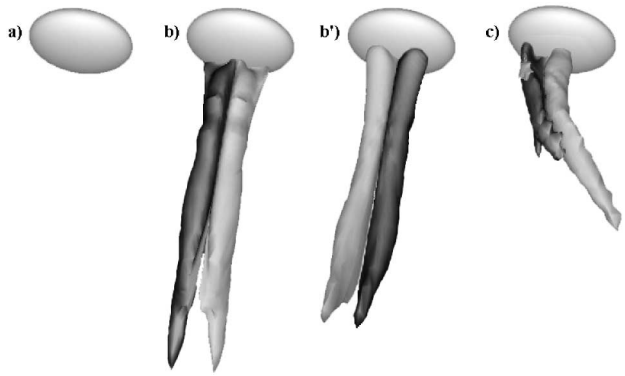

FIG. 5. Isosurfaces $\omega_x(R_{\mathrm{eq}}/g)^{1/2} = \pm 2.7$ of the streamwise vorticity (Ga = 138; the darker thread corresponds to the positive value). (a) $\chi < \chi_c$, rectilinear path; (b) $\chi = 2.50$, zigzag path; (b′) same, half a period later; (c) $\chi = 2.50$, spiral path.

as the most stable configuration, since it is the one in which vorticity can be evacuated with the greatest efficiency.

We note that increasing χ for a given Ga increases the amount of vorticity generated on the bubble and the anisotropy of added-mass coefficients, while maintaining the capacity of the flow to evacuate vorticity at a given level. In contrast, for moderate values of Ga, increasing Ga for a given χ increases the efficiency of both the generation and the evacuation of vorticity, while maintaining the anisotropy of the body constant. Thus, the strength of the two destabilizing mechanisms (vorticity generation and anisotropy of the body) increases during the fixed-Ga transition, while the fixed-χ transition corresponds to an increased strength of the stabilizing mechanism (vorticity evacuation) and of only one of the destabilizing mechanisms. This is probably why the saturated amplitude of the zigzag is much larger for a given value of $(\chi - \chi_c)/\chi_c$ than for the same value of $(\mathrm{Ga} - \mathrm{Ga}_c)/\mathrm{Ga}_c$.

Figure 6 shows the evolution of the bubble Reynolds number $\mathrm{Re} = 2R_{\mathrm{eq}}\|\boldsymbol{U}\|/\nu$ in the case $\mathrm{Ga} = 138$, $\chi = 2.5$. In the rectilinear stage, Re increases regularly up to the value $\mathrm{Re}_1 = 1035$. Then the Reynolds number experiences a sharp drop and oscillates around the value $\mathrm{Re}_2 = 835$ during the zigzag stage. A second drop, leading to the final value $\mathrm{Re}_3 \approx 600$, occurs when the bubble enters the spiral stage. This evolution clearly shows that each of the two path transitions is associated with a large increase of the drag resulting from an increase of the dissipation in the wake. For the particular case shown in Fig. 6, the final drag is about thrice as large as the "steady state" drag corresponding to the end of the rectilinear stage.

The most questionable assumption of our model is undoubtedly that of a constant aspect ratio. Clearly, given the evolution of $\boldsymbol{U}$, the Weber number $\mathrm{We} = \rho U^2 R_{\mathrm{eq}}/\sigma$ (σ denoting surface tension) undergoes a significant drop at each of the two symmetry breakings of the trajectory. Consequently, the oblateness of a real air bubble certainly decreases during each of these transitions. Since the drag coefficient is an increasing function of χ, we guess that this change of shape tends to soften the drag increase described above; it can also delay the corresponding transition by lowering vorticity generation. In contrast, assuming a frozen shape during the zigzag and spiral stages is certainly correct, as shown experimentally in [4]. Another feature agreeing with [4] is the smallness of the instantaneous drift angle β between the minor axis of the bubble and the velocity $\boldsymbol{U}$. In the computations β never exceeds 2°, suggesting that deformations due to transverse motions may indeed be neglected compared to those due to the streamwise velocity.

The results obtained in the present investigation demonstrate that wake instability and anisotropic added-mass effects associated with oblate spheroids suffice to explain path instability of millimetric bubbles rising in low-viscosity liquids. Small-scale deformations which have been totally disregarded here appear to be only a secondary ingredient of the problem. They can probably influence quantitatively most of the characteristics of path instability, but can hardly change the nature of the mechanisms described here. Despite the successful qualitative comparison between the results of the present model and those of available experiments, many points still require careful investigation. For instance, the precise limits of existence of the zigzag and spiral states in the (Ga, χ) plane must be thoroughly specified and the nature of the bifurcations between two successive states must be completely determined. The connection between the marginal curves $\chi_c(\mathrm{Ga})$ of the present problem and the marginal curve $\chi(\mathrm{Re})$ determining the region of wake instability of a spheroidal bubble fixed in the fluid must also be investigated to determine the effect of the additional degrees of freedom due to the free translation and rotation of the body. Finally, it would be highly desirable to derive a simple but realistic model for the rotational force and torque $\boldsymbol{F}_\omega$ and Γ_ω in Eqs. (3), in order to model the whole problem with a system of coupled ODE in the spirit of the heuristic model proposed in [11] for describing the free fall of two-dimensional bodies.

We warmly thank F. Charru and F. Risso for having shared so often our fascination for zigzagging and spiraling bubbles, as well as for all their fruitful suggestions.

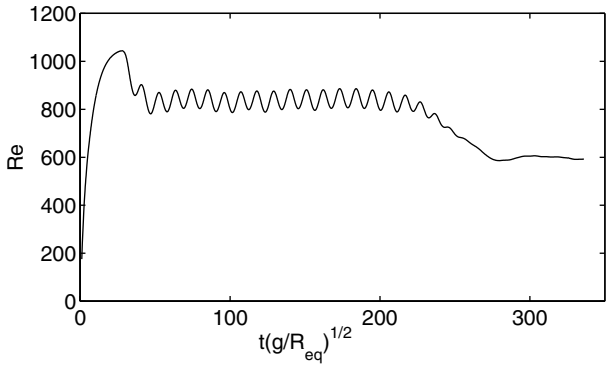

FIG. 6. Time evolution of the bubble Reynolds number ($\mathrm{Ga} = 138$, $\chi = 2.50$).

[1] J. Magnaudet and I. Eames, Annu. Rev. Fluid Mech. **32**, 659 (2000).
[2] P. C. Duineveld, J. Fluid Mech. **292**, 325 (1995).
[3] T. B. Benjamin, J. Fluid Mech. **181**, 349 (1987).
[4] K. Ellingsen and F. Risso, J. Fluid Mech. **440**, 235 (2001).
[5] P. G. Saffman, J. Fluid Mech. **1**, 249 (1956).
[6] A. De Vries, Ph.D. thesis, Twente University, The Netherlands, 2001.
[7] E. Kelley and M. Wu, Phys. Rev. Lett. **79**, 1265 (1997).
[8] G. Mougin and J. Magnaudet, Int. J. Multiph. Flow (to be published).
[9] M. S. Howe, Q. J. Mech. Appl. Math. **48**, 401 (1995).
[10] G. K. Batchelor, *An Introduction to Fluid Dynamics* (Cambridge University Press, Cambridge, United Kingdom, 1967).
[11] L. Mahadevan, C. R. Acad. Sci. Ser. IIb **323**, 729 (1996).